A Novel Surface-Wave-Based High-Impedance Surface Multibeam Antenna With Full Azimuth Coverage

Zi Long Ma, *Member, IEEE*, and Chi Hou Chan, *Fellow, IEEE*

***Abstract*— This paper presents a novel surface-wave (SW)-based high-impedance surface (HIS) multibeam antenna with 360° scanning capability in azimuth. The proposed antenna consists of four rotationally symmetric beamforming networks (BFNs) and a microstrip patch array-based HIS. Regarding to the BFN, it is formed by a planar offset parabolic reflector fed by multiple substrate integrated waveguides. Through proper design, the proposed BFN can efficiently launch guided SWs with TM_0 mode. With the perturbation of the HIS structure, the bounded SWs can be transformed to $m = -1$ space harmonic mode leaky-wave radiation. Combining the feature of the leaky-wave radiation in the elevation plane and the manipulation of the propagation direction of the SWs by switching the feeding ports, beam scanning in the azimuth direction with a tilted elevation angle can be realized. As the HIS is shared by the four BFNs, the size of the antenna can be reduced and a broadened antenna scanning range is achieved. In this paper, a prototype of the proposed antenna with 28 feeding ports, 7 in each BFN, is numerically analyzed and experimentally demonstrated. The proposed antenna features low-cost, low-profile, and single layer configuration.**

***Index Terms*— Beamforming, high-impedance surface (HIS), integrated reflector antenna, multibeam antenna, planar antenna, surface wave (SW).**

I. Introduction

MULTIBEAM antennas are often defined as antennas, which are with capability to form multiple beams in different directions from the same aperture [1]. In recent years, as the rapid development and the growing complexity of telecommunication and surveillance systems, multibeam antenna has received much interest in the electromagnetics community. A typical multibeam antenna is constructed by a beamforming network (BFN) and a corresponding number of radiating elements. As a key part of the entire system, the BFN can tailor the phase and amplitude for the radiators to obtain the required far-field radiation performance. By switching the various input ports, different phase gradients can be provided to the radiators to realize beam steering. For the radiating elements, individual or arrayed radiators are commonly used. In the published works, various types of BFNs can be found. Circuit-based BFNs, such as the Blass, Nolen, and Butler matrix techniques, were discussed in detail in [2]–[4], respectively. Similarly, lens-based BFNs, such as Rotman [5], [6] and Ruze [7] lenses, were reported as w ell. However, these solutions have some major drawbacks, such as bulky in size, high power loss, complicated design process, and so on. Comparatively, the parabolic reflector-based BFN that employed in [8]–[10] provides an easier implementation. It adopts quasi-optical principle and integrates the feeding horns and the parabolic reflector surface on a substrate by using substrate integrated waveguide (SIW) technique. Since the absence of cross-over sections and delay lines, this design has relatively compact size and efficient performance.

In the past decades, studies on surface-wave (SW) issue were widely conducted, because of its intrinsic property that TM_0 mode has no cutoff frequency. The manipulation to SWs was focused on two main aspects, suppression of undesired SWs and radiation by driving the efficiently excited SWs. For the former issue, papers [11] and [12] employed electromagnetic bandgap structures to reduce the SW effects. On the other hand, for the latter, several antenna designs based on SW excitation were presented in [13]–[16]. These antennas based on dielectric slabs exhibit the advantage of low profile. Furthermore, in order to efficiently launch directed SWs, the slot-based Yagi–Uda-type SW launchers were proposed in [17] and [18]. However, these SW launchers may have performance variation within a broad frequency band and result in unstable antenna patterns and gain. In [19], we proposed an integrated parabolic reflector-based SW launcher. Compared with the existing studies, it has more broad operating band. It was employed in an SW-based leaky-wave antenna design, and stable radiation performance was achieved. Several concepts, such as SW guiding structure and SW reflector and focusing system, were discussed in [19] as well.

In this paper, we extend the study in [19] and propose a novel SW-based high-impedance surface (HIS) multibeam antenna with full azimuth coverage. The following problems are addressed in this paper. First, the scanning range of the conventional planar multibeam antenna is broadened. Second, attributed to the configuration that the radiating part (HIS) is shared by the four BFNs, the proposed antenna has a relatively compact size. Furthermore, compared with the published SW-based leaky-wave antennas [15], [16], a more stable and improved radiation performance can be achieved by this paper. The novelties of this paper can be summarized as:

Manuscript received June 13, 2016; revised December 8, 2016; accepted January 15, 2017. Date of publication February 16, 2017; date of current version April 5, 2017.

The authors are with the State Key Laboratory of Millimeter Waves, Partner Laboratory in City University of Hong Kong, Hong Kong (e-mail: zilongma@cityu.edu.hk; eechic@cityu.edu.hk).

Color versions of one or more of the figures in this paper are available online at http://ieeexplore.ieee.org.

Digital Object Identifier 10.1109/TAP.2017.2670320

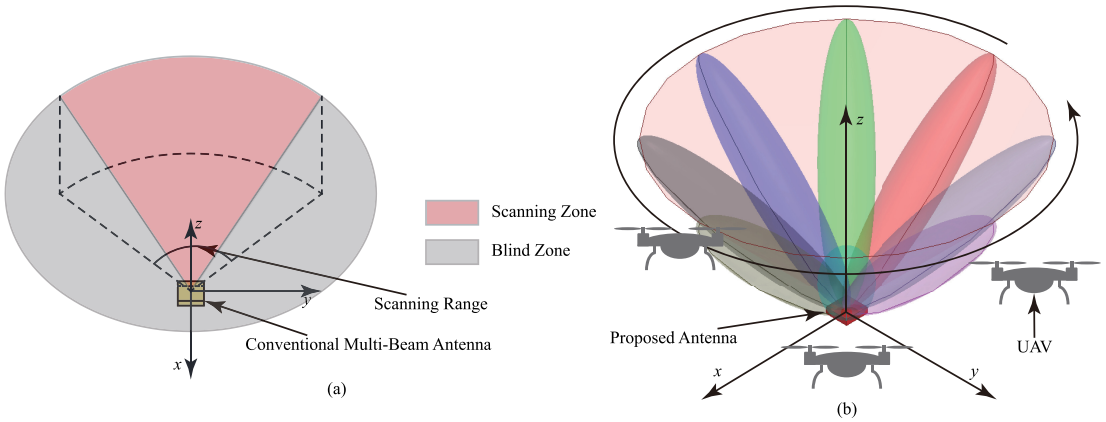

Fig. 1. Illustrations of (a) scanning range of the conventional multibeam antennas and (b) scanning range and potential UAV surveillance application of the proposed antenna.

1) we propose a novel antenna structure in which SW is applied to multibeam antenna design, where integrated offset parabolic reflectors are adopted to SW excitation and 2) to the best of the our knowledge, this is the first time a full azimuth scanning multibeam antenna with tilted elevation angle in a planar configuration is proposed. The proposed antenna features low-cost, low-profile, and single layer configuration.

This paper is organized as follows. In Section II, we describe the problem that needs to be solved in this paper and discuss the potential applications of the proposed antenna. Section III introduces the antenna configuration. In Section IV, the operation and design principles are presented. The dispersion analyses of the HIS and design procedure for the proposed antenna are provided. In Section V, experimental results of a prototype of the proposed antenna with 28 feeding ports, 7 in each BFN, are illustrated. Finally, a conclusion can be found in Section VI.

II. Problem Statements and Potential Application

In the existing literature, the studies of multibeam antennas are often focused on 1-D scanning issues. Typically, the scanning planes are either broadside or end-fire. However, as we know that the modern antenna systems are often required to operate in complicated environments where objects appear at different locations with respect to the antenna system. The locations of the objects are not only limited in the broadside or end-fire planes. Based on this fact, the studies of multibeam antennas are extended to scanning in a tilted plane with an elevation angle. In [9] and [10], two antennas with this kind of function were proposed. However, from the demonstrated results, the maximum scanning ranges of the two proposed antennas are only within $\pm 45^\circ$ in azimuth. In various practical applications, multibeam antennas with broadened azimuth scanning range will be beneficial to cover more objects and adapt to complicated application scenarios. Furthermore, as aforementioned, in order to produce multiple beams by switching the feeding ports, many different techniques were developed, such as Blass, Nolen and Butler matrices, Rotman and Ruze lenses, and so on. However, similar to [9] and [10], a single BFN that employed one of these techniques can only steer the beams within the range of $\pm 45^\circ$. Due to their intrinsic natures, the scanning ranges are difficult to be further extended. Although Luneburg lens can realize 360° beam steering, it is still not a preferred option in the multibeam system due to its nonplanar configuration and bulky size. In Fig. 1(a), we illustrate the scanning range of the conventional multibeam antennas. The red and gray regions stand for the scanning and blind zones, respectively. Thanks to the well-developed leaky-wave theory, conventional antennas can easily realize beam scanning in elevation. However, for azimuth, it can be seen that except for the small region in the $-x$ direction, most area cannot be covered by conventional designs. Therefore, how to extend the azimuth scanning range of the multibeam antenna is a challenging and practically significant problem.

In designing the proposed full azimuth coverage antenna, the basic idea is to arrange four identical conventional BFNs in a square configuration. Each BFN can control the beams to steer within one quadrant (90°), and then by switching the BFNs, 360° scanning can be realized. The integrated parabolic reflector system can be employed as the BFN in this design due to its aforementioned advantages. However, when we designed the radiating part, a problem arose that the conventional radiators are not suitable for this design, because they are very difficult to receive waves from the four BFNs. For example, the SIW-based slot arrays used in [5], [8], and [10]. The conductive vias will block the waves fed from the orthogonal directions. Therefore, the full azimuth scanning function cannot be realized by simply combining four conventional multibeam designs. Based on this, we design a square microstrip patch-based HIS as the radiating part. By employing the concept of SW, the power from the four BFNs can be successfully transmitted to the HIS. Since the proposed HIS is a symmetric structure, the far-field beams will not be distorted by the switching of the BFNs. Compared with the existing multibeam antenna array that proposed in [5], the proposed antenna has more compact size and low profile.

The proposed antenna can be applied to various surveillance radar systems because of its beam steering feature and 2-D conical scanning pattern. Specifically, one potential application

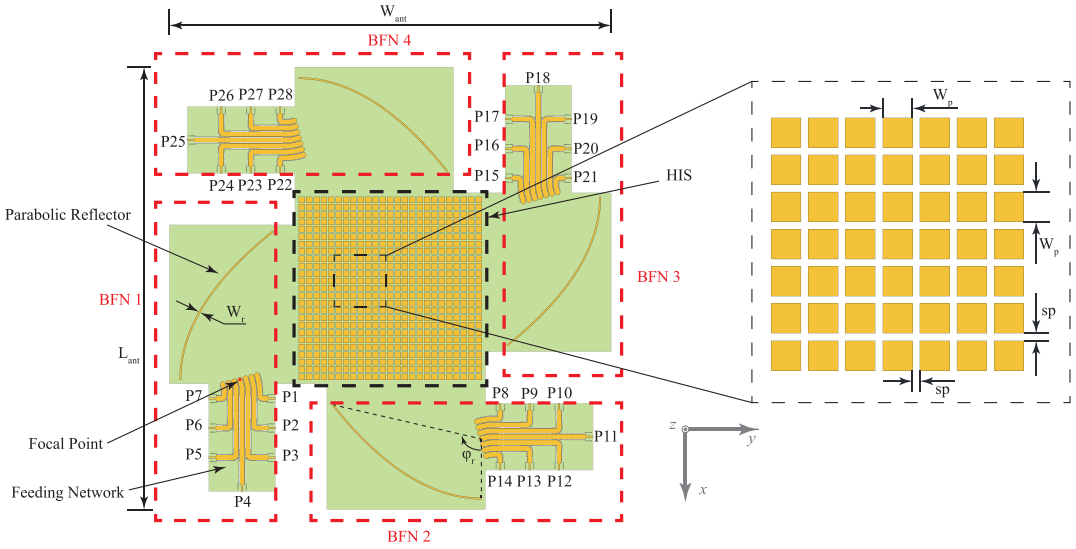

Fig. 2. Overall configuration of the proposed antenna. The red and black dashed lines indicate the BFNs and HIS, respectively.

can be unmanned aerial vehicle (UAV) surveillance radar system. The application scenario is shown in Fig. 1(b). It can be seen that the proposed antenna can transmit radar signals toward all azimuth directions. Once the UAVs enter into the surveillance area, they can be detected in time. This application can avoid the security issues brought by the ever-increasing number of UAVs. It should be mentioned that although the conventional conical beam antennas may also be used in this application, the proposed antenna will have better positioning ability due to its beam switching function. On the other hand, as we know that multibeam antennas often produce directional beams with narrow beamwidths. In order to obtain large coverage or high scanning resolution, a large number of feeding ports have to be used [4], [20]. In the proposed design, we employ 28 feeding ports for the antenna. Although the number of the ports is large, the design is practical and the performance of the entire antenna system will not be affected. In the specific implementation, we can use single-pole multithrow switches to realize the switchings between the various ports. The connections between the proposed antenna and the front-end system can also be simplified correspondingly. In addition, this paper aims to investigate the main performances of the proposed antenna. The prototype with 28 feeding ports is designed for demonstration. In practical applications, the number of feeding ports can be properly adjusted to meet different requirements. The design principle is universal.

In this paper, the proposed antenna can be regarded as a fixed frequency design for the following reasons. First, the main purpose of this paper is to investigate the azimuth scanning capability of the proposed antenna. Its scanning performance in elevation is not a main discussion in this paper. Second, for the proposed antenna, the beam steering in elevation mainly depends on the leaky-wave principle. To change the beam directions, the operating frequency should be varied. However, the use of frequency converter will increase the cost of the entire system. Third, from Fig. 1(b), we can see that the proposed antenna needs to have a fixed elevation angle to determine the surveillance area. The beam scanning in the elevation plane is not a necessary capability for the potential surveillance radar application.

III. Antenna Configuration

The overall configuration of the proposed antenna and the coordinate system is presented in Fig. 2. It can be observed that the proposed antenna consists of four identical BFNs and a 25×25 microstrip patch array-based HIS. The four BFNs are arranged in a rotationally symmetric fashion and the HIS structure is placed in the center region. Regarding to each BFN, it includes a planar offset parabolic reflector surface and an SIW-based feeding network with seven input ports. The parabolic reflector surface is directly carved from the grounded dielectric substrate and it is metalized by copper. The ends of the seven SIW feeds are linearly arranged and Port 4 feeds the reflector at its focal point. Once any one port is excited, SW can be generated from the corresponding output port of the feeding network, and then guided along the substrate. The reflector surface can redirect and reshape the SWs. The HIS structure plays a role of the radiating part. In Fig. 2, the red and black dashed lines indicate the BFNs and HIS, respectively. The port numbers are also indicated at different feeding positions. It should be mentioned that the substrate selection is a key consideration in designing the proposed antenna. As described in [21], a thicker substrate and higher dielectric constant will be easier to generate SWs. Therefore, a laminate, with permittivity $\epsilon_r = 10.2$, dissipation factor $\tan\delta = 0.0035$, and substrate thickness $h = 62$ mil, is used in this design.

IV. Operation and Design Principles

A. Design of Beamforming Network

The BFN is composed by an offset parabolic reflector surface and an SIW feeding network. Therefore, we can

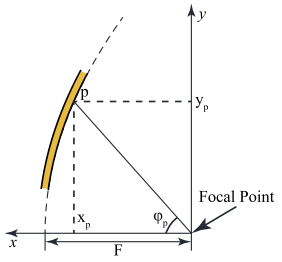

Fig. 3. Illustration of the design of the offset-fed parabolic reflector surface.

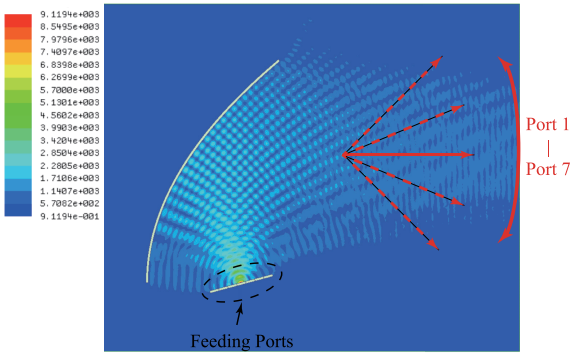

Fig. 4. Full-wave simulated E-field distribution of the SW launched by Port 4 and an illustration of the operation principle of the proposed antenna (unit: V/m). The solid and dashed straight line arrows indicate the propagation directions of the SWs launched by Port 4 and other feeding ports, respectively.

separately design the two parts. For the parabolic reflector, the analysis can be performed from the perspective of ray-optics. The basic principle is to make the path length of each ray starting from the focal point to a given wavefront perpendicular to the propagation direction of the reflected ray be identical. In other words, a cylindrical wave from a source located at the focal point can be transformed to a collimated fashion by the reflector surface. Fig. 3 shows the design of the offset-fed parabolic reflector surface. An arbitrary point on the surface is denoted as p and the focal point is at the origin of the coordinate. The reflected waves propagate in the $-x$ direction. The parabolic reflector surface can be described by

$$\begin{cases} x_p = \dfrac{2F}{1+\cos\phi_p}\cos\phi_p \\ y_p = \dfrac{2F}{1+\cos\phi_p}\sin\phi_p \end{cases} \tag{1}$$

where x_p and y_p are the positions of point p. ϕ_p stands for the angle of point p with the x-axis. F is the focal length.

In order to investigate the performance of the parabolic reflector with the SW, a full-wave simulation is performed in Ansys HFSS. Fig. 4 presents the full-wave simulated E-field distribution of the SW launched by Port 4. In this simulation, the feeding network is replaced by seven waveports defined in HFSS and the TM_0 mode SW is excited. We can see that the excited SW can be guided by the grounded dielectric substrate. After the reflector, the waves are reshaped. This result demonstrates that the SW can be successfully guided by the selected dielectric substrate and the manipulation to the

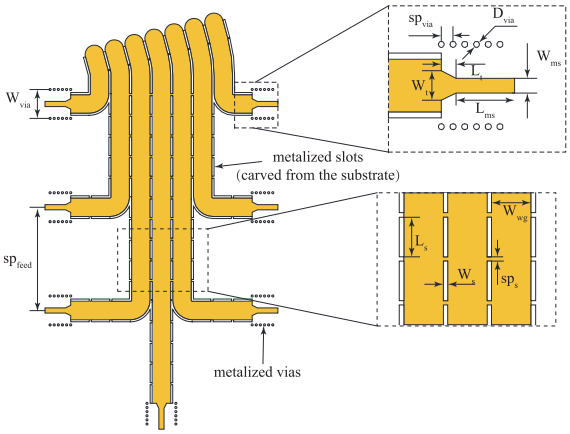

Fig. 5. Configuration of the proposed feeding network.

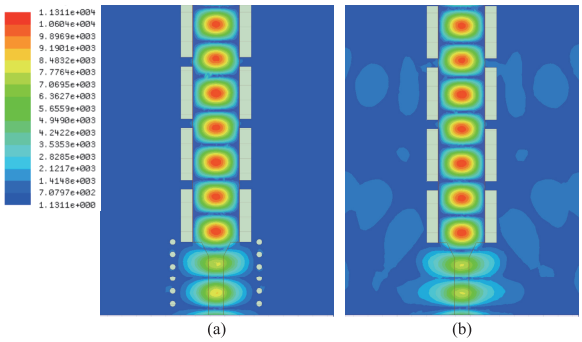

Fig. 6. Full-wave simulated E-fields of the microstrip to SIW transition (a) with and (b) without the metalized vias (unit: V/m).

SW by using the planar reflector is feasible. In Fig. 4, a simple illustration of the azimuth scanning principle is also provided. By switching the various feeding ports, the propagation direction of the reflected waves will be changed accordingly. As a result, the radiation beam in the far-field region can be steered.

For the feeding network, the detailed configuration is presented in Fig. 5. The basic design method comes from the conventional SIW technique. However, during the design process, we found the via-based configuration increases the computation time and affects the final convergence. Therefore, the vias in conventional design are replaced by the metalized slots (carved from the substrate) as shown in Fig. 5. The gap size sp_s between the adjacent slots still obeys the SIW design rules. The length L_s can be selected flexibly. In addition, the proposed antenna adopts an edge feed. A linearly tapered transition from a microstrip line to the SIW is designed. The detailed design method can be found in [22]. On the two sides of the transition part, metalized vias are designed to prevent the SW leakage. A comparison of the E-field distributions with and without the vias is presented in Fig. 6. It can be seen that the vias can confine the SWs very well. In this paper, each SIW supports the fundamental TE_{10} mode.

Fig. 7 shows simulated vector E-field distribution of the TM_0 mode SW launched by the proposed BFN. It can be observed that the E-field direction is perpendicular to the xy plane. Note that the design principle of F, ϕ_r, and

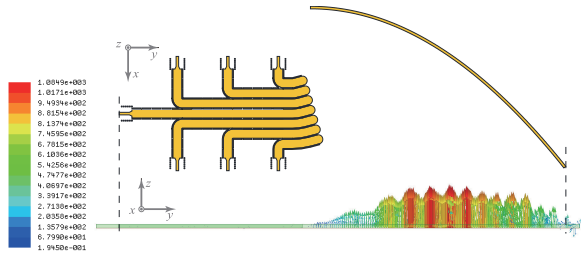

Fig. 7. Full-wave simulated vector E-field of the TM_0 mode SW launched by the proposed BFN (unit: V/m).

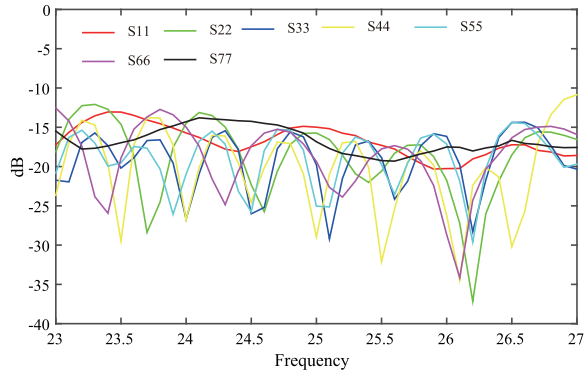

Fig. 8. Simulated impedance matchings of the proposed BFN.

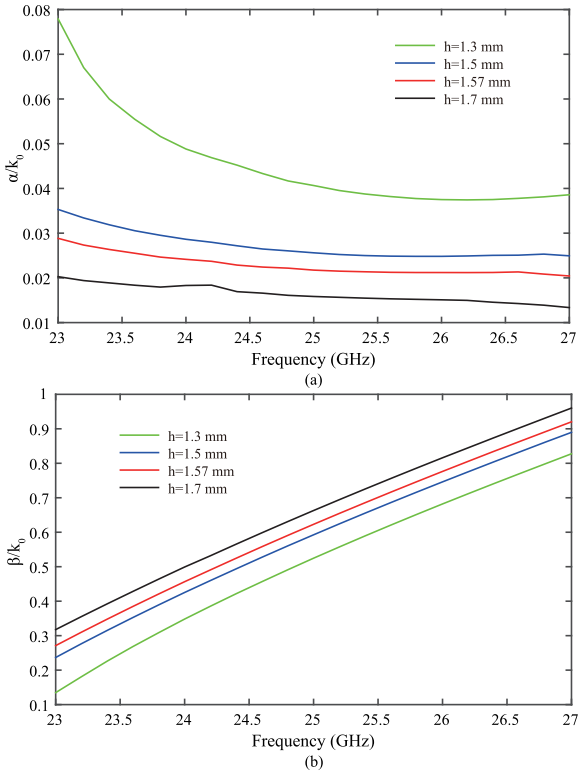

Fig. 9. Dispersion relations of the proposed HIS structure for various substrate thicknesses h ($W_p = 4$ mm and $sp = 1$ mm). (a) Attenuation constants. (b) Phase constants.

orientation of the SIWs is similar to that of conventional offset parabolic reflectors, which can be found from [23]. The simulated impedance matchings of the proposed BFN are presented in Fig. 8.

It is worth mentioning that in the practical environment, the loss of the proposed antenna mainly comes from ohmic loss, dielectric loss, and SW attenuation. The former two kinds of losses commonly exist in various antennas. For the latter, as mentioned in [17], almost all of the SW attenuation is due to the imperfect dielectric. We can reduce it by using high-quality dielectric material. For the losses of the feeding network, we can roughly estimate the efficiency of the feeding network from the simulated S-parameters. In this simulation, we remove the HIS structure. Two identical BFNs are arranged in a face-to-face manner and separated by a small distance (2 mm). One BFN is excited from the port, which is located at the focal point (Port 4) and the same port of the other BFN is used to collect the transmitted power. Since the two BFNs are the same, the efficiency of a single BFN can be estimated by $|S_{21}|/2$. Due to the small separation distance, the SW attenuation in the dielectric slab is ignored. From the calculation, the efficiency of the BFN is almost 76%. Because of the two BFNs are very close, a small portion of waves may be disorderly reflected by the parabolic reflectors. It may cause unnecessary but unavoidable power loss in the simulation. Therefore, the efficiency of the proposed BFN should be greater than 76%.

B. Design of High-Impedance Surface

Since the HIS needs to receive the SWs from the four BFNs, square-shaped microstrip patches should be the best option. We can consider a lossless situation that the SW propagation direction is normal to the HIS cross section. Due to the periodic configuration, the Floquet theory can be applied. The expression of the phase constant can be found

$$\beta_m(\omega) = \pm\left[\beta_{sw}(\omega) + \frac{2m\pi}{W_p + sp}\right] \quad m = 0, \pm1, \pm2, \pm3 \ldots\ldots \tag{2}$$

where m refers to the mode index. β_{sw} is the phase constant of the SW. For the proposed antenna, the $m = -1$ space harmonic mode is excited to realize leaky-wave radiation. The main beam direction θ (angle from broadside direction) can be approximated by [24]

$$\theta \approx \sin^{-1}(\beta_{-1}(\omega)/k_0). \tag{3}$$

In order to design the HIS, dispersion analyses are performed. In Figs. 9 and 10, the effects of the substrate thickness h and the patch spacing sp on the dispersion relations are presented, respectively. All the dispersion relations are extracted from the full-wave simulation and the method can be found in [25]. It can be observed that with the decrease of h and the increase of sp, the attenuation constants are gradually increased. A high attenuation constant means that the excited SWs are with a loosely bound status and more energy can be radiated to the far-field region. At the same time, by changing the two parameters (h and sp), the phase constants are varied as well, and as a result, the beam angle in elevation will be changed. When designing such an HIS, our design goal is to

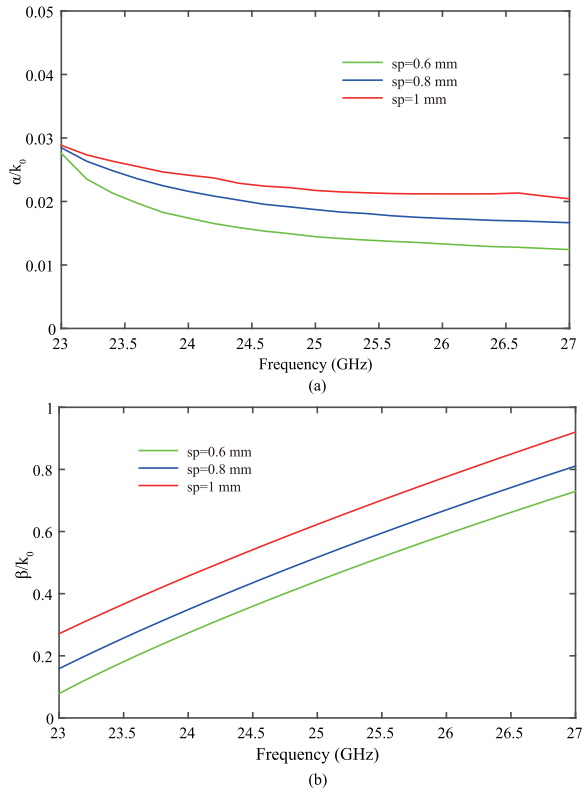

Fig. 10. Dispersion relations of the proposed HIS structure for various microstrip patch spacings sp ($W_p = 4$ mm and $h = 62$ mil). (a) Attenuation constants. (b) Phase constants.

make the excited SWs be radiated as much as possible so that the proposed antenna can achieve high radiation intensity. Therefore, a high attenuation constant is preferred. At the same time, the discussions on the phase constants will be helpful for fine-tuning the beam angle. In this design, the substrate thickness $h = 1.57$ mm (62 mil) is chosen as this is the typical thickness of commercially available laminate. In practical applications, this substrate thickness can be customized. The design of the parameter W_p can be easily determined by the leaky-wave theory, namely, (2) and (3). We can see that the parameter W_p dominates the variation of the phase constant. The change of W_p will lead to a downward or upward shift of the phase constant in a frequency band. Since the proposed antenna operates in the forward radiation region, at a fixed frequency, a large W_p will result in a large beam angle θ and vice versa. In designing the HIS, we can properly tune the value of W_p to meet the requirement of the beam angle in elevation. Note that in Fig. 9, when the parameter h is varied, $W_p = 4$ mm and $sp = 1$ mm, while, in Fig. 10, the parameter sp is varied with $W_p = 4$ mm and $h = 62$ mil. It should be noted that the dispersion analyses discussed here are for the case that the SW propagation direction is normal to the HIS cross section. For the entire antenna system, it maps to the excitations from Ports 4, 11, 18, and 25. For the other ports, the variation trends of the dispersion relations should be similar and the design principles are still remain valid. These discussions provide a design guideline for the proposed HIS.

Based on the above-mentioned discussions, the final geometrical parameters of the proposed antenna can be obtained.

TABLE I
GEOMETRICAL PARAMETERS (IN mm AND rad)

L_{ant}	W_{ant}	W_r	F	W_{via}	sp_{feed}	sp_{via}
300	300	1	40	6	20	0.85
D_{via}	W_t	L_t	L_{ms}	W_{ms}	W_p	sp
0.4	2	1	4	1	4	1
ϕ_r	L_s	W_s	W_{wg}	sp_s		
$\frac{4\pi}{7}$	3.6	0.4	3.2	0.6		

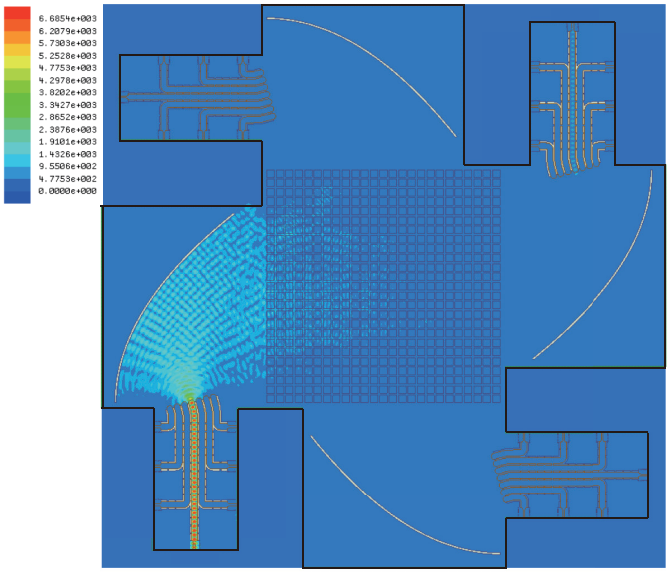

Fig. 11. Full-wave simulated E-field distribution on the whole antenna when Port 4 is excited (unit: V/m).

They are listed in Table I. The E-field distribution on the entire antenna is investigated and presented in Fig. 11. We can see that when Port 4 is excited, only a small portion of fed power is transmitted to Port 18. It demonstrates that the isolation between the two ports is at a relatively high level. Based on this, it can be deduced that the coupling between BFN 1 and BFN 3 should be low. In Fig. 12, the simulated 3-D radiation patterns of the proposed antenna excited by BFN 1 (Ports 1–7) are presented. Beam steering in azimuth direction can be clearly observed by switching the feeding ports. Since the four BFNs are identical and the structure is symmetric, the radiation patterns excited by the other BFNs should have similar azimuthal variation.

V. EXPERIMENTAL DEMONSTRATION

A prototype of the proposed antenna with center frequency $f_0 = 25$ GHz is fabricated and tested. In Fig. 13, photographs of the prototype and the measurement setup are presented. In the measurement, we design and fabricate an extra aluminum fixture to support the prototype and fix the connectors. The prototype is mounted on this metal fixture by using the screws. In addition, a 3-D printed fixture is also fabricated to connect the metal fixture and the measurement system. The radiation performance of the proposed antenna is measured in Nearfield Systems Inc. near-field measurement system.

The simulated and measured impedance matchings of the BFN 1 of the proposed antenna are shown in Fig. 14.

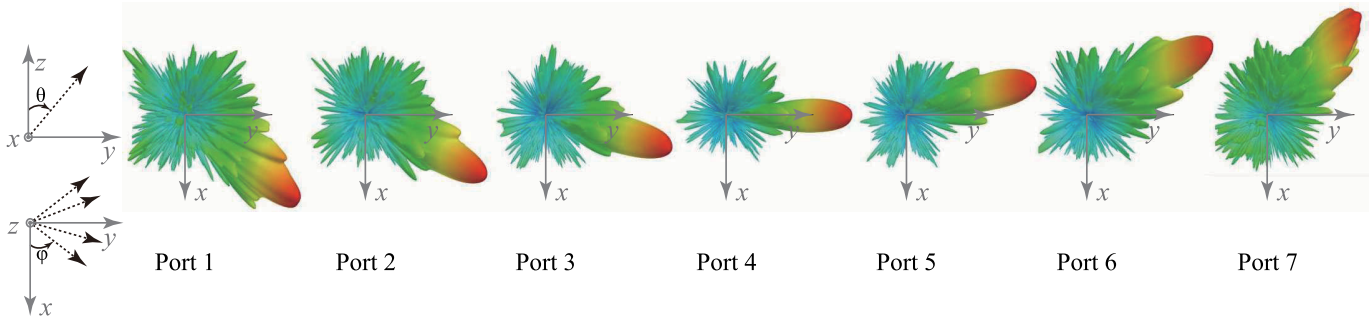

Fig. 12. Full-wave simulated 3-D radiation patterns of the proposed antenna excited from Ports 1 to 7.

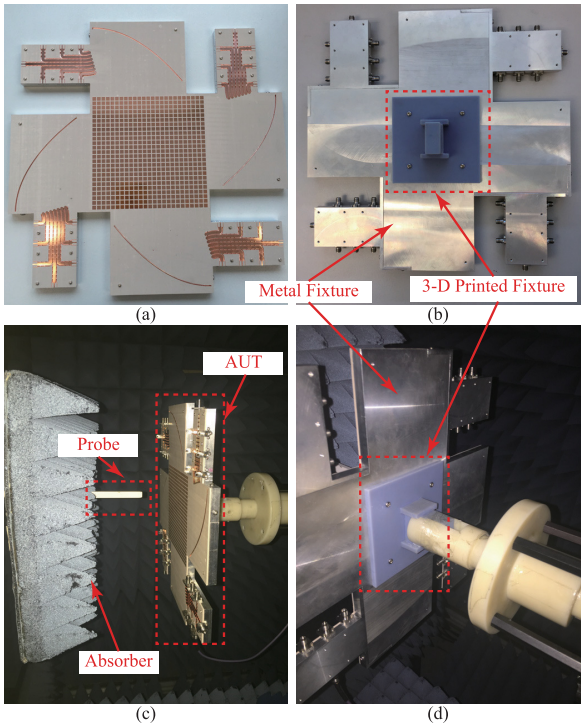

Fig. 13. Photographs of the fabricated antenna prototype and the measurement setup. (a) Top and (b) bottom views of the prototype. (c) Front and (d) back views of the measurement setup.

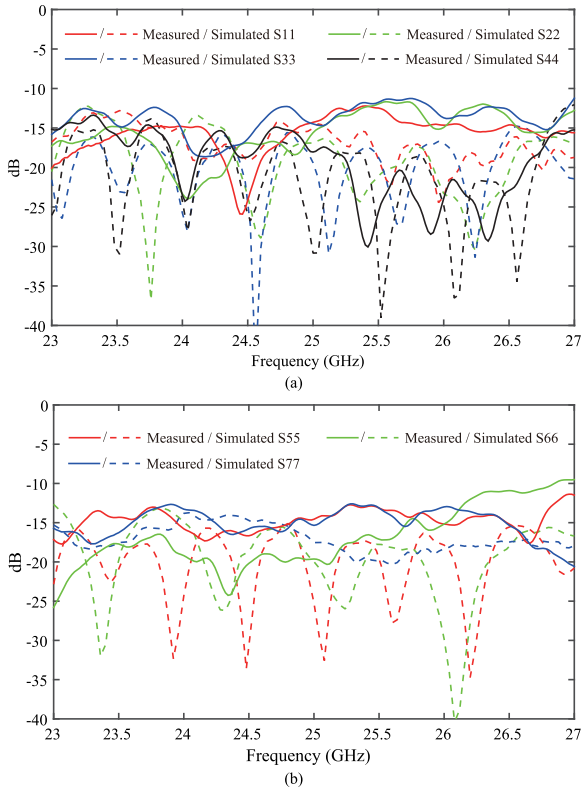

Fig. 14. Measured and simulated impedance matchings of BFN 1 of the proposed antenna. (a) Ports 1–4. (b) Ports 5–7.

Within the frequency band 23–27 GHz, all the feeding ports are matched. At the center frequency f_0, the reflection coefficients are all below -10 dB. The small discrepancies between the measured and simulated results may come from the difference between the ideal situation in simulation and practical implementation as well as the effects of the used connectors.

It is well known that for the multiport devices, the mutual coupling issues should always be considered. In this design, due to the symmetry reason, the mutual couplings can be categorized into three types, namely: 1) the couplings between any two ports in BFN 1; 2) the couplings between any two ports, one each in BFN 1 and BFN 2; and 3) the couplings between any two ports, one each in BFN 1 and BFN 3. For Type 1, the couplings are low due to the existence of the SIW boundaries. A similar validation can be found from [8]. In addition, from a physical perspective, the couplings of Type 2 should be very low as well. Because the propagation directions of the SWs excited by these two BFNs are almost orthogonal, the waves are difficult to propagate between them. Based on this rule, Type 3 couplings should be designed carefully, because of the face-to-face configuration of BFN 1 and BFN 3. In Fig. 15, the measured and simulated mutual couplings between Ports 4 and 18 are presented. The measured $|S_{4,18}|$ shows a flat trend and is below -28 dB within 23–27 GHz. The trends of the simulated and measured results are the same. The small discrepancy may be caused by the imperfection of the practical laminate. Similar discrepancy can be found in [26]. Since the proposed antenna is a fixed frequency design, the measured mutual couplings of the various port pairs are listed in Table II. We can see that the measured maximum couplings of the three types are -29.7, -36.1, and -27.4 dB, respectively. They correspond to $|S_{1,2}|$, $|S_{1,14}|$, and $|S_{6,20}|$.

TABLE II
MEASURED MUTUAL COUPLINGS BETWEEN VARIOUS FEEDING PORTS AT CENTER FREQUENCY (UNIT: dB)

	Port 1	Port 2	Port 3	Port 4	Port 5	Port 6	Port 7	Port 8	Port 9	Port 10	Port 11
Port 1	–	−29.7	−37.3	−38	−40.4	−51.3	−37.2	−48.6	−63.4	−56.7	−52
Port 2	–	–	−34.4	−37.2	−41.4	−36.5	−50	−53.5	−61.5	−57	−54.9
Port 3	–	–	–	−34.1	−37.8	−37.5	−40.2	−57.4	−65.1	−59.6	−58.5
Port 4	–	–	–	–	−33.5	−35.1	−37.1	−60.9	−60.8	−70.5	−69.6
Port 5	–	–	–	–	–	−33.1	−35.8	−58	−55.4	−63.8	−59.9
Port 6	–	–	–	–	–	–	−31.2	−55.3	−55.2	−58	−64.2
Port 7	–	–	–	–	–	–	–	−60.1	−64.8	−68.5	−59.5
	Port 12	Port 13	Port 14	Port 15	Port 16	Port 17	Port 18	Port 19	Port 20	Port 21	
Port 1	−50.1	−44.4	−36.1	−33.2	−34.6	−42.4	−49.7	−61.8	−59.4	−50.2	
Port 2	−54.3	−57.3	−45.1	−34.3	−31.8	−37.4	−45.2	−53.9	−59.3	−57.4	
Port 3	−60.6	−62.3	−56.6	−43.2	−37.2	−31.1	−42.5	−54.9	−49	−54.7	
Port 4	−73.8	−61.4	−62.9	−51.7	−47.6	−42.1	−29	−43.9	−54.8	−54.3	
Port 5	−62.3	−71.2	−54.6	−61.8	−50.3	−58	−43.6	−29.4	−39.5	−47.6	
Port 6	−60.9	−65.8	−57.8	−68.9	−62.9	−48.5	−55	−39.3	−27.4	−40.8	
Port 7	−61.3	−73.2	−65.9	−50.5	−57	−55	−51.7	−48.4	−41.6	−27.5	

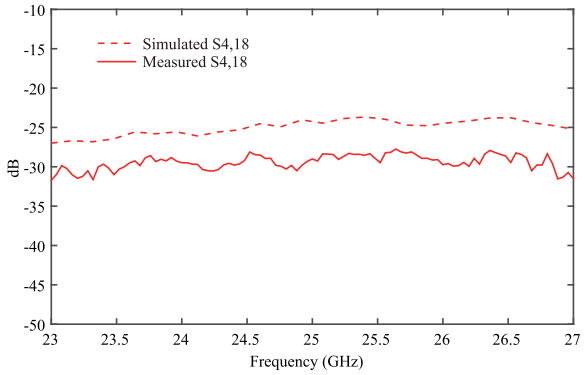

Fig. 15. Measured and simulated mutual couplings between Ports 4 and 18.

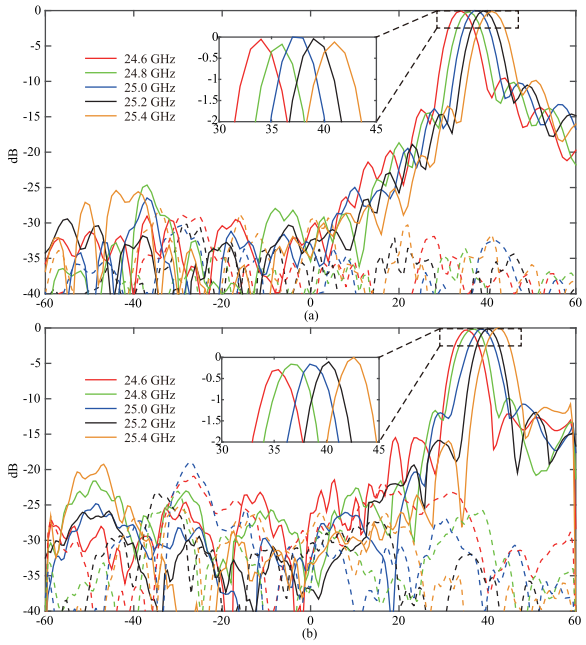

Fig. 16. (a) Simulated and (b) measured E-plane radiation patterns for Port 4. The solid and dashed lines stand for the copolarization and cross-polarizations, respectively.

Fig. 16 shows the simulated and measured copolarized and cross-polarized E-plane radiation patterns when Port 4 is excited. It can be seen that the simulated and measured

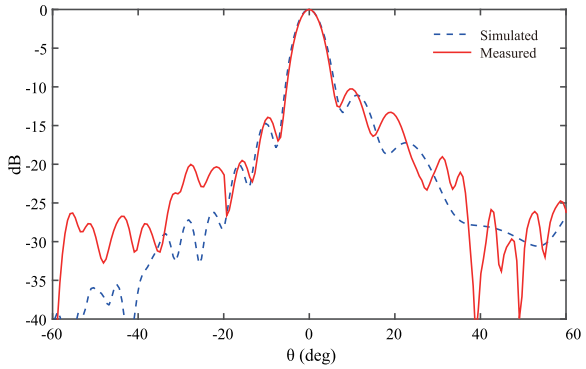

Fig. 17. Simulated and measured H-plane radiation patterns at f_0 for Port 4. The coordinate system is rotated with respect to the x-axis. The point $\theta = 0°$ is at the maximum radiation direction.

results show reasonable agreements. Due to the leaky-wave characteristic, the measured main beam is steered from 35.4° to 42.6° in elevation direction within the frequency band 24.6–25.4 GHz. All the simulated and measured results are normalized to the maximum value of all patterns, respectively. We can see that the scan losses are small. From the measured results, the scan losses are smaller than 0.5 dB. In Fig. 17, the simulated and measured H-plane radiation patterns at f_0 excited at Port 4 are compared. They exhibit good agreement. It should be noted that because the main beam is with a tilted elevation angle at f_0 with respect to the original coordinate system in Fig. 2, the present H-plane coordinate system is rotated with respect to the x-axis and the point $\theta = 0°$ is at the maximum radiation direction. The cross-polarization levels of Ports 1–7 at center frequency are −8.3, −10.2, −15.7, −36.7, −15.1, −9.8, and −11.4 dB, respectively. The increase of the cross-polarized radiation is mainly caused by the tilted incidence of the SW. We can see that if the incident angle of the SW is normal to the HIS, namely, the antenna is excited at Port 4, and the cross-polarization is very small. With the variation of the SW incident angle, the cross-polarization level tends to increase. The further the incident angle deviates from the normal direction, the larger the cross-polarization. From the leaky-wave theory, we know that the slots that are transverse to the SW propagation direction mainly contribute

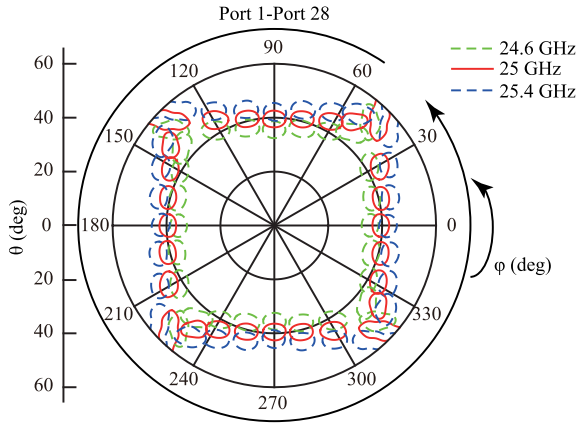

Fig. 18. Measured 3-dB beamwidth contour radiation patterns at {24.6, 25, 25.4} GHz for Ports 1–28. The patterns of Ports 8–28 are replicated from those of Ports 1–7 because of the symmetry of the proposed antenna.

TABLE III

MEASURED BEAM DIRECTIONS OF THE PROPOSED ANTENNA EXCITED FROM BFN 1 (ϕ AND θ)

	24.6 GHz	25 GHz	25.4 GHz
Port 1	(+48°,+45.6°)	(+53.4°,+47.4°)	(+52.8°,+51.6°)
Port 2	(+59.4°,+40.2°)	(+61.8°,+43.8°)	(+63°,+47.4°)
Port 3	(+73.8°,+37.2°)	(+75°,+40.8°)	(+76.2°,+44.4°)
Port 4	(+89.4°,+35.4°)	(+90°,+40.2°)	(+90°,+42.6°)
Port 5	(+105.6°,+37.8°)	(+103.8°,+40.8°)	(+103.8°,+44.4°)
Port 6	(+121.8°,+41.4°)	(+119.4°,+44.4°)	(+117°,+48°)
Port 7	(+136.2°,+52.2°)	(+136.2°,+57°)	(+127.2°,+53.4°)

to the copolarized radiation. The tilted SW may illuminate the orthogonal slots and increase the cross-polarization level. This problem is an unavoidable physical limitation and commonly happens in most phased array antennas. However, since the proposed design is mainly for surveillance radar applications, the cross-polarized radiation will not affect the performance of the entire system. It is because the operating principle of the surveillance radar is based on the reflections of electromagnetic waves and the polarization status of the reflected waves is often changed by the complicated structure of the object.

In Fig. 18, the measured 3-dB beamwidth contour radiation patterns at 24.6, 25, and 25.4 GHz for Ports 1–28 are presented. The patterns of Ports 8–28 are replicated from those of Ports 1–7 because of the symmetry of the proposed antenna. The measured beam directions for BFN 1 are listed in Table III. We can see that for a single BFN, the main beam scanning ranges are 88.2°, 82.8°, and 74.4° at 24.6, 25, and 25.4 GHz, respectively. The 3-dB beamwidth can almost cover 90°. Therefore, through switching the twenty eight feeding ports (four BFNs), 360° beam scanning in azimuth direction can be realized. In Fig. 19, the measured and simulated antenna gain for various feeding ports in BFN 1 are presented. The trends of the measured and the simulated results are similar. The measured gain is a bit lower than the simulated results. The average discrepancy between the simulation and measurement is almost 3.2 dB. The discrepancy may be caused by the fabrication tolerance and the imperfection of the used laminate. At 24.6, 25, and 25.4 GHz, the differences between

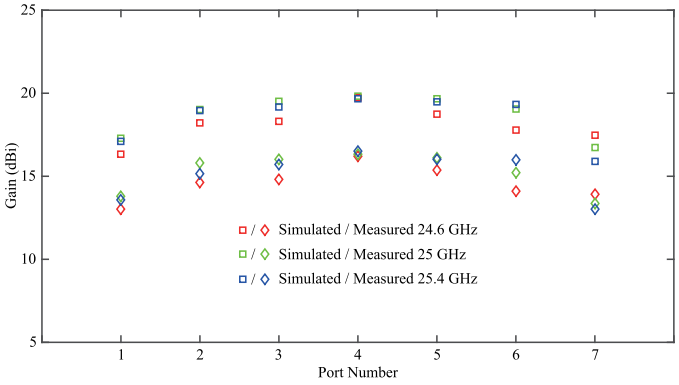

Fig. 19. Measured and simulated gain for various feeding ports in BFN 1 at {24.6, 25, 25.4} GHz.

the measured maximum and minimum gain are 3.02, 3, and 3.5 dB for various feeding ports, respectively. It is worth mentioning that the beamwidth of the proposed antenna in the E- and H-plane can be independently adjusted. The leaky-wave theory controls the beamwidth variation in the E-plane. At the same time, H-plane patterns are dominated by the BFN. By properly choosing the physical dimensions (F and ϕ_r) of the reflector surface, the small gaps between the adjacent patterns in Fig. 18 can be bridged. The present prototype aims to investigate the main characteristics and performances of the proposed antenna. Fine-tuning of the antenna parameters is not the goal of this paper. On the other hand, in Fig. 18 and Table III, beam direction variations in elevation by switching the feeding ports can be found. This phenomenon is caused by oblique incidence of the SWs to the HIS. The detailed descriptions can be found in [9].

The aperture efficiencies of the proposed antenna for Ports 1–7 are 18%, 28%, 36%, 40%, 36%, 28%, and 17%, respectively. The low aperture efficiencies are because the proposed HIS needs to fit to the SWs in various directions. In order to make the SWs from every direction be radiated efficiently, the proposed HIS has to be increased in area. Although the proposed antenna has relatively low aperture efficiencies, this is a performance tradeoff between the aperture efficiencies and the function of full azimuth scanning. In order to realize the full azimuth coverage, a portion of aperture efficiency has to be sacrificed. For a large or full azimuth coverage application, we may use a conventional method that several separate multibeam antennas are employed to form an array. However, this method may increase the system size, design complexity, and power loss. In contrast, the proposed antenna has advantages of low cost, low profile, and ease of fabrication. From this aspect, although the aperture efficiencies are relatively low, the proposed antenna is still a good option for large or full azimuth coverage applications.

VI. CONCLUSION

In this paper, a novel SW-based HIS multibeam antenna with full azimuth coverage has been proposed. A prototype of the proposed antenna with 28 feeding ports, 7 in each BFN, has been successfully demonstrated. The proposed

antenna employs SW excitation and leaky-wave principle. The TM_0 mode SW can be efficiently launched by the proposed BFN and transformed to $m = -1$ space harmonic mode leaky-wave radiation. By switching the various feeding ports, beam scanning in azimuth direction with a tilted elevation angle has been realized. The proposed antenna has broadened scanning range and relatively compact size. It features low-cost, low-profile, and single layer configuration.

REFERENCES

[1] P. S. Hall and S. J. Vetterlein, "Review of radio frequency beamforming techniques for scanned and multiple beam antennas," *IEE Proc. H-Microw. Antennas Propag.*, vol. 137, no. 5, pp. 293–303, Oct. 1990.

[2] S. Mosca, F. Bilotti, A. Toscano, and L. Vegni, "A novel design method for Blass matrix beam-forming networks," *IEEE Trans. Antennas Propag.*, vol. 50, no. 2, pp. 225–232, Feb. 2002.

[3] T. Djerafi and N. J. G. Fonseca, "Planar Ku-band 4×4 Nolen matrix in SIW technology," *IEEE Trans. Microw. Theory Techn.*, vol. 58, no. 2, pp. 259–266, Feb. 2010.

[4] P. Chen *et al.*, "A multibeam antenna based on substrate integrated waveguide technology for MIMO wireless communications," *IEEE Trans. Antennas Propag.*, vol. 57, no. 6, pp. 1813–1821, Jun. 2009.

[5] Y. J. Cheng *et al.*, "Substrate integrated waveguide (SIW) Rotman lens and its Ka-band multibeam array antenna applications," *IEEE Trans. Antennas Propag.*, vol. 56, no. 8, pp. 2504–2513, Aug. 2008.

[6] W. Lee, J. Kim, and Y. J. Yoon, "Compact two-layer Rotman lens-fed microstrip antenna array at 24 GHz," *IEEE Trans. Antennas Propag.*, vol. 59, no. 2, pp. 460–466, Feb. 2011.

[7] J. Ruze, "Wide-angle metal-plate optics," *Proc. IRE*, vol. 38, no. 1, pp. 53–69, Jan. 1950.

[8] Y. J. Cheng, W. Hong, and K. Wu, "Millimeter-wave substrate integrated waveguide multibeam antenna based on the parabolic reflector principle," *IEEE Trans. Antennas Propag.*, vol. 56, no. 9, pp. 3055–3058, Sep. 2008.

[9] M. Ettorre, R. Sauleau, and L. L. Coq, "Multi-beam multi-layer leaky-wave SIW pillbox antenna for millimeter-wave applications," *IEEE Trans. Antennas Propag.*, vol. 59, no. 4, pp. 1093–1100, Apr. 2011.

[10] Y. J. Cheng, W. Hong, K. Wu, and Y. Fan, "Millimeter-wave substrate integrated waveguide long slot leaky-wave antennas and two-dimensional multibeam applications," *IEEE Trans. Antennas Propag.*, vol. 59, no. 1, pp. 40–47, Jan. 2011.

[11] D. Sievenpiper, L. Zhang, R. F. J. Broas, N. G. Alexopolous, and E. Yablonovitch, "High-impedance electromagnetic surfaces with a forbidden frequency band," *IEEE Trans. Microw. Theory Techn.*, vol. 47, no. 11, pp. 2059–2074, Nov. 1999.

[12] N. Llombart, A. Neto, G. Gerini, and P. de Maagt, "Planar circularly symmetric EBG structures for reducing surface waves in printed antennas," *IEEE Trans. Antennas Propag.*, vol. 53, no. 10, pp. 3210–3218, Oct. 2005.

[13] A. Al-Zoubi, F. Yang, and A. Kishk, "A low-profile dual-band surface wave antenna with a monopole-like pattern," *IEEE Trans. Antennas Propag.*, vol. 55, no. 12, pp. 3404–3412, Dec. 2007.

[14] M. Li, S. Q. Xiao, Z. Wang, and B. Z. Wang, "Compact surface-wave assisted beam-steerable antenna based on HIS," *IEEE Trans. Antennas Propag.*, vol. 62, no. 7, pp. 3511–3519, Jul. 2014.

[15] S. K. Podilchak, A. P. Freundorfer, and Y. M. M. Antar, "Surface-wave launchers for beam steering and application to planar leaky-wave antennas," *IEEE Trans. Antennas Propag.*, vol. 57, no. 2, pp. 355–363, Feb. 2009.

[16] S. K. Podilchak, L. Matekovits, A. P. Freundorfer, Y. M. M. Antar, and M. Orefice, "Controlled leaky-wave radiation from a planar configuration of width-modulated microstrip lines," *IEEE Trans. Antennas Propag.*, vol. 61, no. 10, pp. 4957–4972, Oct. 2013.

[17] A. R. Perkons, Y. Qian, and T. Itoh, "TM surface-wave power combining by a planar active-lens amplifier," *IEEE Trans. Microw. Theory Techn.*, vol. 46, no. 6, pp. 775–783, Jun. 1998.

[18] H. F. Hammad, Y. M. M. Antar, A. P. Freundorfer, and S. F. Mahmoud, "Uni-planar CPW-fed slot launchers for efficient TM_0 surface-wave excitation," *IEEE Trans. Microw. Theory Techn.*, vol. 51, no. 4, pp. 1234–1240, Apr. 2003.

[19] Z. L. Ma, "Dispersion engineering of periodic structures and its applications to antenna designs," Ph.D. dissertation, Dept. Elect. Electron. Eng., Univ. Hong Kong, Hong Kong, 2015.

[20] *EHF Rotman Lens Fed Linear Array Multibeam Planar Near-Field Range Measurements*, accessed on Jun. 10, 2016. [Online]. Available: https://www.cst.com/Content/Events/nauf2008/06-maybell.pdf

[21] D. M. Pozar, "Microstrip antennas," *Proc. IEEE*, vol. 80, no. 1, pp. 79–91, Jan. 1992.

[22] D. Deslandes, "Design equations for tapered microstrip-to-substrate integrated waveguide transitions," in *IEEE MTT-S Int. Microw. Symp. Dig.*, Anaheim, CA, USA, May 2010, p. 704.

[23] A. W. Rudge and N. A. Adatia, "Offset parabolic-reflector antennas: A review," *Proc. IEEE*, vol. 66, no. 12, pp. 1592–1623, Dec. 1978.

[24] A. A. Oliner and D. R. Jackson, "Leaky-wave antennas," in *Antenna Engineering Handbook*, J. Volakis, Ed., 4th ed. New York, NY, USA: McGraw-Hill, 2007, ch. 10.

[25] C. Caloz and T. Itoh, *Electromagnetic Metamaterials, Transmission Line Theory and Microwave Applications*. New York, NY, USA: Wiley, 2005.

[26] J. Liu, D. R. Jackson, and Y. Long, "Substrate integrated waveguide (SIW) leaky-wave antenna with transverse slots," *IEEE Trans. Antennas Propag.*, vol. 60, no. 1, pp. 20–29, Jan. 2012.

Zi Long Ma (M'15) received the B.S. degree from the South China University of Technology, Guangzhou, China, in 2010, and the M.S. and Ph.D. degrees from The University of Hong Kong, Hong Kong, in 2011 and 2015, respectively, all in electrical and electronic engineering.

From 2011 to 2015, he was with the Center of Electromagnetics and Optics, The University of Hong Kong. Since 2014, he has been with the State Key Laboratory of Millimeter Waves, Partner Laboratory in City University of Hong Kong, Hong Kong, where he is currently a Post-Doctoral Fellow. His current research interests include periodic structures, leaky-wave antennas, composite right/left handed structures, multibeam antennas, millimeter-wave antennas, and RFID antennas.

Dr. Ma received the Best Student Paper Award (Second Prize) in Progress in Electromagnetics Research Symposium in 2014. He served as a Reviewer of the IEEE TRANSACTIONS ON ANTENNAS AND PROPAGATION, the IEEE TRANSACTIONS ON MICROWAVE THEORY AND TECHNIQUES, the *IEEE Antennas and Wireless Propagation Letters*, and the *IET Microwaves, Antennas and Propagation*.

Chi Hou Chan (S'86–M'86–SM'00–F'02) received the B.S. and M.S. degrees from The Ohio State University, Columbus, OH, USA, in 1981 and 1982, respectively, and the Ph.D. degree from the University of Illinois at Urbana–Champaign, Champaign, IL, USA, in 1987, all in electrical engineering.

From 1987 to 1989, he was a Visiting Assistant Professor with the Department of Electrical and Computer Engineering, University of Illinois at Urbana–Champaign. From 1989 to 1998, he was a Faculty Member with the Department of Electrical Engineering, University of Washington, Seattle, WA, USA. In 1996, he joined the Department of Electronic Engineering, City University of Hong Kong, Hong Kong, and was promoted to the Chair Professor of Electronic Engineering in 1998. From 1998 to 2009, he was first an Associate Dean and then the Dean of the College of Science and Engineering. He also served as an Acting Provost of the University from 2009 to 2010. He is currently the Director of State Key Laboratory of Millimeter Waves, Partner Laboratory in City University of Hong Kong, Hong Kong. His current research interests include computational electromagnetics, millimeter-wave circuits and antennas, and terahertz science and technology.

Dr. Chan is the General Co-Chair of ISAP 2010, iWAT 2011, iWEN 2013, ICCEM 2015, ICCEM 2016 and GSMM 2017.